Backup Transmission Line Protection for Ground Faults and Power Swing Detection Using Synchrophasors

Armando Guzmán, Venkat Mynam, and Greg Zweigle
Schweitzer Engineering Laboratories, Inc.

Backup Transmission Line Protection for Ground Faults and Power Swing Detection Using Synchrophasors

Armando Guzmán, Venkat Mynam, Greg Zweigle, *Schweitzer Engineering Laboratories, Inc.*

Abstract—This paper proposes the use of synchrophasors for backup transmission line protection for ground faults and power swing detection. The proposed protection approach complements protective distance elements and is suitable for single-pole and three-pole tripping applications. The paper presents the synchrophasor-based protective element performance for challenging fault conditions such as cross-country faults with high fault resistance. The power swing detection algorithm this paper proposes uses angle difference measurements and does not require setting traditional impedance-based out-of-step (OOS) characteristics.

Keywords—Negative, Zero, Sequence, Current, Angle, Difference, Frequency, Slip, Acceleration, Swing, Out-of-Step

I. INTRODUCTION

Synchrophasors within protective relays have been available since 2002. Typical applications of this technology are visualization, state measurement, and system integrity protection schemes.

Relays that combine synchrophasor measurements and programmable logic control capabilities [1] use synchrophasor measurements from both ends of a two-terminal transmission line to provide backup protection and power system stability monitoring (see Fig. 1). The backup protection uses negative- or zero-sequence current elements to detect high fault resistance (R_F) faults. Operating times for these elements depend on the synchrophasor message rate and the synchrophasor filtering process. In the present implementation, the sequence component-based backup protection elements detect faults with R_F greater than 300 Ω within 160 ms. This current only element R_F coverage compares to negative-sequence impedance-based directional elements [2], 67Q, but does not require voltage measurements. These elements include faulted phase identification (FPI) logic that makes them suitable for single-pole tripping (SPT) applications.

These relays also gather positive-sequence voltage angle measurements from two different power system buses. With these measurements, the relays determine the angle difference [3] between the two buses and calculate the slip frequency and acceleration to identify power swings and OOS conditions.
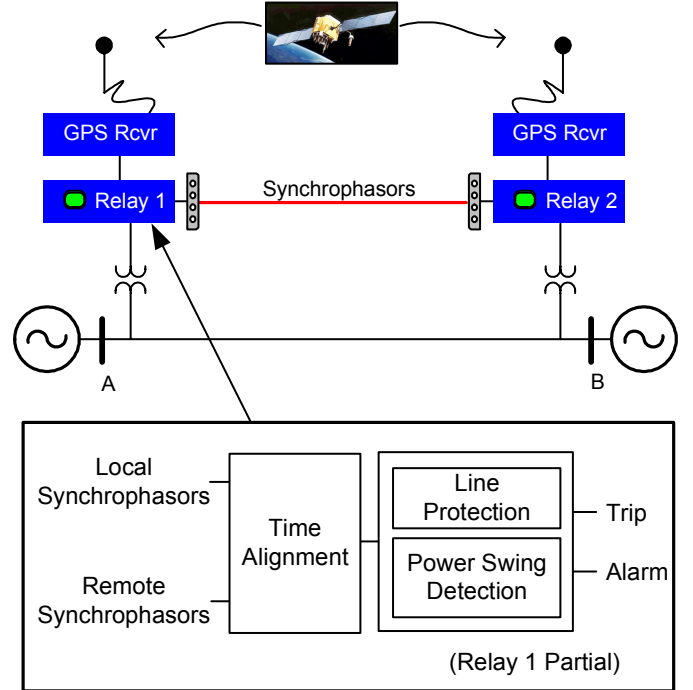

Fig. 1. Relays Exchange Synchrophasors for Backup Line Protection and Power System Detection in a Two-Terminal Line Application.

II. BACKUP TRANSMISSION LINE PROTECTION

Line protective relays calculate synchrophasors at specific instants (60 times per second, for example). Communications channels make the local and remote time-stamped currents available to the local and remote relays. These relays time align the local and remote currents on a per phase basis and make them available to protective functions (see Fig. 2) such as FPI logic, negative-sequence current directional element (32IQ), zero-sequence current directional element (32IG), negative-sequence current differential element (87LQ), and zero-sequence current differential element (87LG).
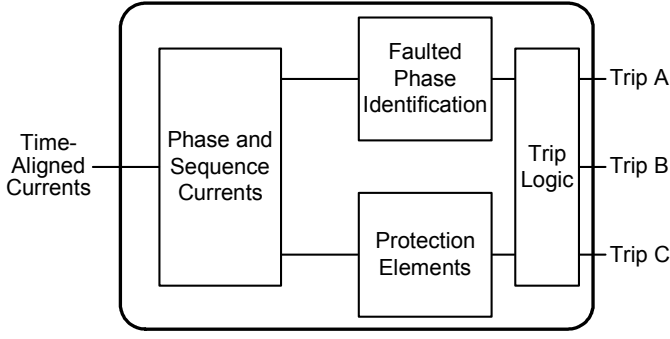
Fig. 2. Synchrophasor-Based Protection Including Phase Currents, Sequence Currents, Faulted Phase Identification Logic, Protection Elements, and Trip Logic.

A. Faulted Phase Identification (FPI)

The synchrophasor-based protection element includes FPI logic that uses the total zero-sequence and total negative-sequence fault currents [4]. The total currents are the sum of the local and remote currents. The logic in Fig. 3 defines sectors FSA, FSB, and FSC corresponding to A-phase, B-phase, and C-phase faults respectively. The logic calculates the angle difference between the sequence fault currents and the relative magnitudes of the total phase-to-phase currents to identify the faulted phase:

A-Phase Fault. The logic asserts the FSA bit

$$\text{if } -60^0 < \left(\angle \mathbf{I}_0^T - \angle \mathbf{I}_2^T\right) \le 60^0 \text{ and}$$

$$\left|\mathbf{I}_{BC}^T\right| \neq \max\left(\left|\mathbf{I}_{AB}^T\right|, \left|\mathbf{I}_{BC}^T\right|, \left|\mathbf{I}_{CA}^T\right|\right)$$

B-Phase Fault. The logic asserts the FSB bit

$$\text{if } 60^0 < \left(\angle \mathbf{I}_0^T - \angle \mathbf{I}_2^T\right) \le 180^0 \text{ and}$$

$$\left|\mathbf{I}_{CA}^T\right| \neq \max\left(\left|\mathbf{I}_{AB}^T\right|, \left|\mathbf{I}_{BC}^T\right|, \left|\mathbf{I}_{CA}^T\right|\right)$$

C-Phase Fault. The logic asserts the FSC bit

$$\text{if } -180^0 < \left(\angle \mathbf{I}_0^T - \angle \mathbf{I}_2^T\right) \le -60^0 \text{ and}$$

$$\left|\mathbf{I}_{AB}^T\right| \neq \max\left(\left|\mathbf{I}_{AB}^T\right|, \left|\mathbf{I}_{BC}^T\right|, \left|\mathbf{I}_{CA}^T\right|\right)$$

where

$\mathbf{I}_0^T$ is the total zero-sequence current phasor

$\mathbf{I}_2^T$ is the total negative-sequence current phasor

$\mathbf{I}_{AB}^T$ is the total A-phase minus B-phase current phasor

$\mathbf{I}_{BC}^T$ is the total B-phase minus C-phase current phasor

$\mathbf{I}_{CA}^T$ is the total C-phase minus A-phase current phasor

The relay uses FPI logic for tripping the faulted phase in SPT applications.

B. Negative-Sequence Current Directional Element (32IQ)

The 32IQ element compares the angle of $\mathbf{I}_2^L$ with the angle of $\mathbf{I}_2^R$ and makes the trip decision according to (1). This element detects high-impedance faults when the negative-sequence currents enter the transmission line at both line ends.

$$\text{Re}\left[\mathbf{I}_2^L \bullet \left(\mathbf{I}_2^R\right)^*\right] > 0 \tag{1}$$

where

$\mathbf{I}_2^L$ is the local negative-sequence current phasor

$\mathbf{I}_2^R$ is the remote negative-sequence current phasor

Fig. 4 shows the basic logic for 32IQ. The Protection Enable bit, PREN, asserts when $\left|\mathbf{I}_2^L\right|$ and $\left|\mathbf{I}_2^R\right|$ exceed the element sensitivity threshold, e.g., $0.1 \bullet I_{NOM}$, and when $\left|\mathbf{I}_2^L\right|$ is greater than $0.05 \bullet \left|\mathbf{I}_1^L\right|$, where $\mathbf{I}_1^L$ is the local positive-sequence current phasor. Communications channel health, data integrity, and time synchronization also supervise this logic. The 32IQ output asserts when all the previous conditions are valid for two consecutive counts.
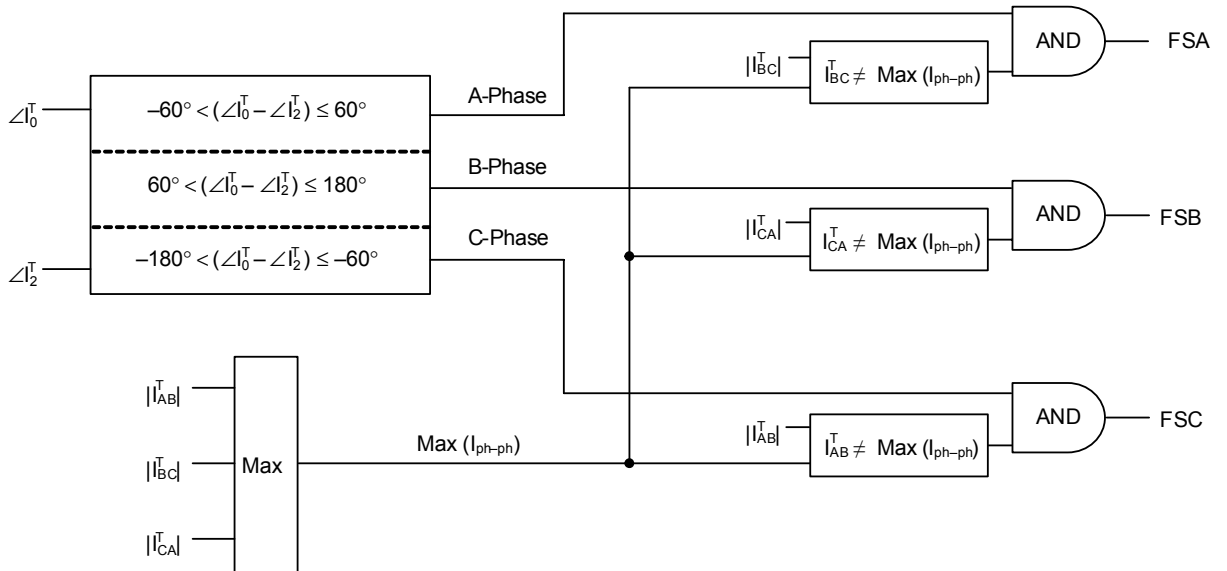

Fig. 3. Faulted Phase Identification Logic Uses Total Negative-Sequence and Zero-Sequence Fault Current.
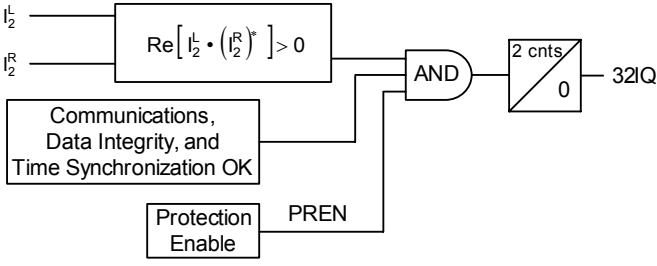
Fig. 4.   Negative-Sequence Current Directional Element, 32IQ, With Current Magnitude, Channel Health, Data Integrity, and Time Synchronization Supervision.

The 32IG element operates similarly to 32IQ but uses zero-sequence quantities.

C. Negative-Sequence Current Differential Element (87LQ)

The 87LQ element characteristic uses operating ($\mathbf{I}_2^{OP}$) and restraint ($\mathbf{I}_2^{RT}$) quantities [5] according to (2) and (3).

$$\mathbf{I}_2^{OP} = \left| \mathbf{I}_2^{L} + \mathbf{I}_2^{R} \right| \tag{2}$$

$$\mathbf{I}_2^{RT} = \left| \mathbf{I}_2^{L} - \mathbf{I}_2^{R} \right| \tag{3}$$

The element operates when the following conditions are met:

$$\mathbf{I}_2^{OP} > 87\_Slope \cdot \mathbf{I}_2^{RT} \tag{4}$$

$$\mathbf{I}_2^{OP} > 0.1 \cdot \mathbf{I}_{NOM} \tag{5}$$

where 87_Slope is the slope of the 87LQ element characteristic.

The relay aligns the local and remote phasors according to their time stamps. Therefore, one advantage of using time-stamped phasors is that channel asymmetry does not affect the element operating and restraint quantities.

The 87LG element operates similarly to 87LQ but uses zero-sequence quantities.

III. PROTECTION ELEMENT PERFORMANCE

A. Fault Resistance Coverage

The 32IQ and 87LQ elements overcome the R_F coverage limitations of traditional phase comparison line protection schemes [6]. Fig. 6 illustrates the R_F coverage of the 67Q, 32IQ, and 87LQ elements for phase-to-ground faults at different fault locations along the transmission line of the system in Fig. 5. We used the Real-Time Digital Simulator (RTDS®) to model this system. For this case, we set element sensitivities to 0.1 • I_{NOM}. The 32IQ and 87LQ R_F coverage matches the intersection of the local and remote 67Q coverage. In a permissive overreaching transfer trip (POTT) scheme with forward and reverse elements, the scheme must coordinate forward and reverse 67Q element sensitivities. The 32IQ and 87LQ elements do not have this requirement, so we can set them more sensitive than 67Q elements. Fig. 7 shows the additional R_F coverage of 32IQ and 87LQ with 0.05 • I_{NOM} sensitivity.
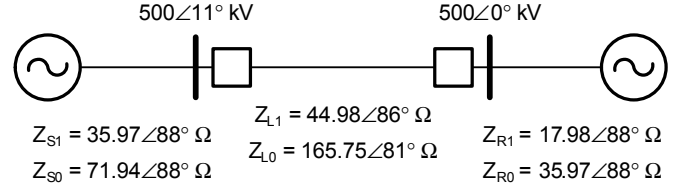

All impedances are in primary ohms

Fig. 5.   Power System Parameters and Operating Conditions to Analyze R_F Coverage Capabilities of the 32IQ, 87LQ, and 67Q Elements.
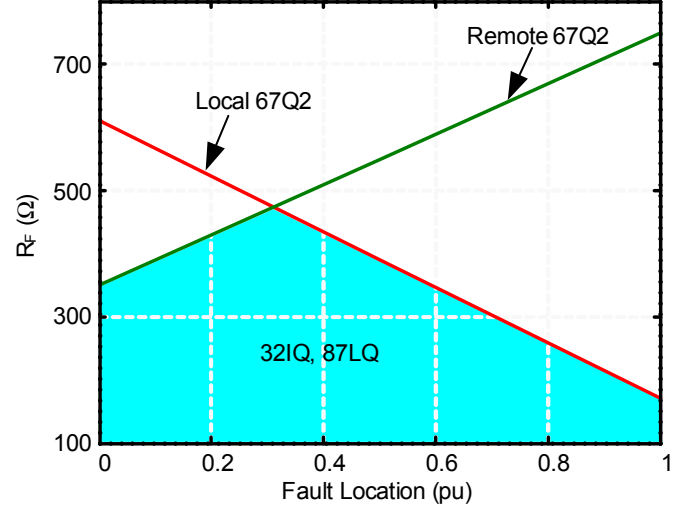

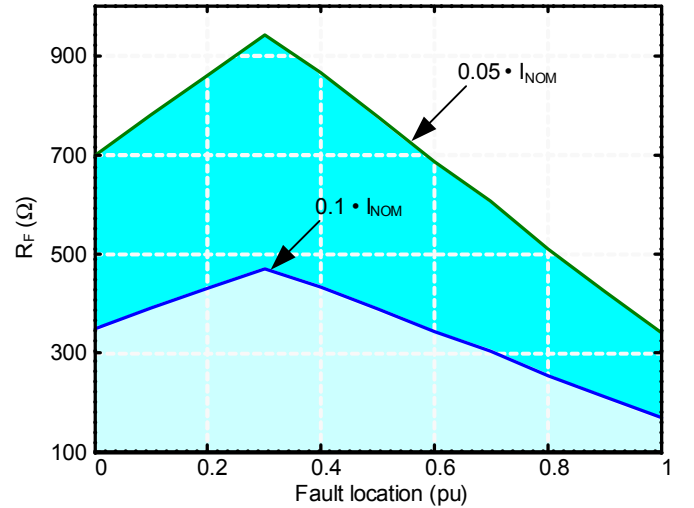Fig. 6.   32IQ, 87LQ, and 67Q Element R_F Coverage for Phase-to-Ground Faults at Different Line Locations.

Fig. 7.   32IQ and 87LQ R_F Coverage With 0.05 • I_{NOM} and 0.1 • I_{NOM} Sensitivity.

B. Operating Time

The operating time of the directional elements depends on the synchrophasor message rate, the synchrophasor filtering process, and element sensitivity. Fig. 8 shows 32IQ element operating time for an A-phase-to-ground-fault with $R_F = 450\ \Omega$ located 30 percent from the local end (left) for the system in Fig. 5. The local and remote relays operate in 165 ms and 158 ms, respectively. In this application, the relays exchange synchrophasors at 20 messages per second, and the filtering system attenuates harmonics according to C37.118

[7]. We set the sensitivity to $0.1 \cdot I_{NOM}$. The relays exchange I_A, I_B, and I_C synchronized phasors along with their corresponding synchronized time stamps through the use of peer-to-peer relay communications [8] at 38400 bps. A faster message rate and faster filtering process reduce element operating time.
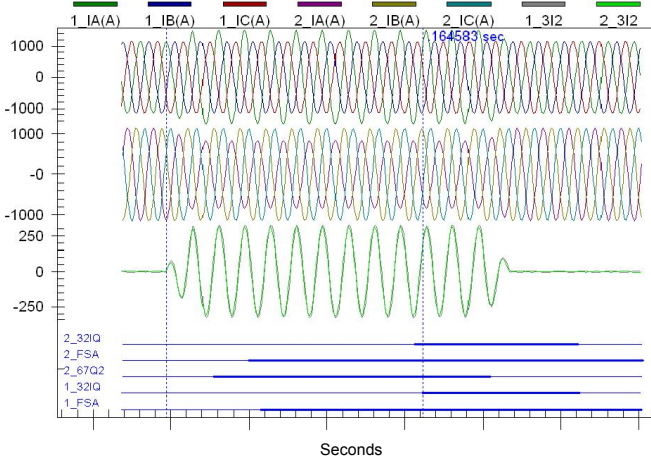

Fig. 8.   FPI, 32IQ, and 67Q Operating Times for an A-Phase-to-Ground Fault Located 30 Percent From the Local End.

C. Effect of Standing Unbalance and Line Loading

Standing negative-sequence current reduces 32IQ R_F coverage [9]. First, consider an A-phase-to-ground fault with $R_F = 350\ \Omega$ located 80 percent from the local end (left) on one of the parallel lines of the system in Fig. 9 during balanced prefault system operating conditions. The prefault negative-sequence current unbalance is zero (see Table I). Fig. 10 shows the local and remote negative-sequence current phasors for this fault. The angle difference between these phasors is 5°. The 32IQ element operates correctly for this fault.

TABLE I.
LOCAL AND REMOTE NEGATIVE-SEQUENCE CURRENTS FOR AN A-PHASE-TO-GROUND FAULT WITH BALANCED PREFAULT CONDITIONS

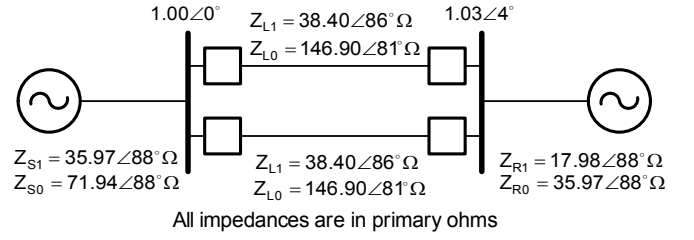| Current	I_2^L (Primary Amps)	I_2^R (Primary Amps)
Prefault	0	0
Fault	57∠0º	92 ∠ −5º

Fig. 9.   Power System Parameters and Operating Conditions to Analyze 32IQ and 87LQ Element Performance For Balanced and Unbalanced Prefault Operating Conditions.
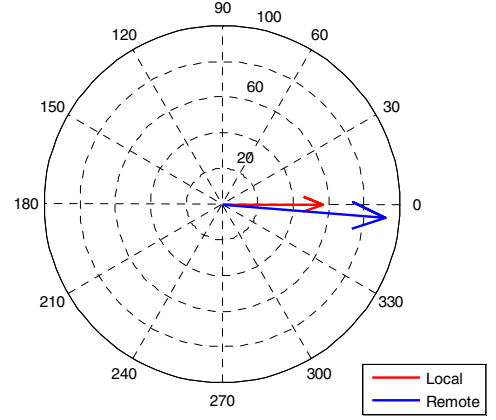

Fig. 10.   Local and Remote Negative-Sequence Currents for an A-Phase-to-Ground Fault Located 80 Percent From the Local End on One of the Parallel Lines With Balanced Prefault Conditions.

Next, we apply the same fault while the A-phase of the parallel line is open. Table II shows the prefault and fault currents. The phasor diagram in Fig. 11 illustrates the load component and the fault without load component together with the fault current at the local and remote terminals. Note that the angle difference between the local and remote fault currents is 108º. This angle difference increases as the load current increases. The 32IQ element does not detect this fault. This element has decreased sensitivity because of the increase in load current for this unbalanced operating condition. In the next subsection, we show that 87LQ and 67Q have greater sensitivity than 32IQ for these operating conditions.

TABLE II.
LOCAL AND REMOTE NEGATIVE-SEQUENCE CURRENTS FOR AN A-PHASE-TO-GROUND WITH UNBALANCED PREFAULT CONDITIONS

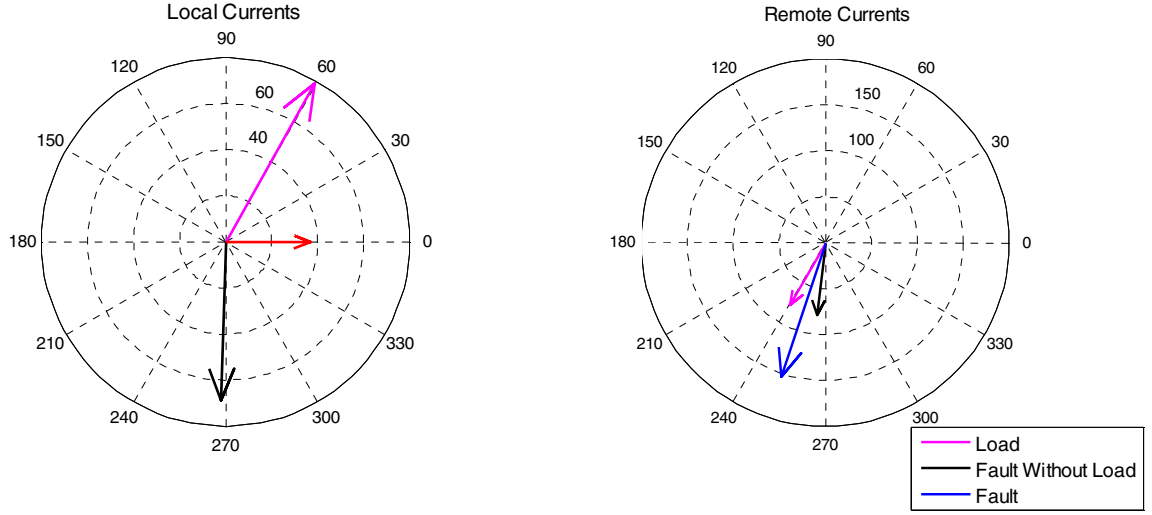| Current	I_2^L (Primary Amps)	I_2^R (Primary Amps)
Prefault	79 ∠ 61º	78 ∠ −119º
Fault	37 ∠ 0º	154 ∠ −108º

Fig. 11.   Local and Remote Negative-Sequence Currents for an A-Phase-to-Ground Fault Located 80 Percent From the Local End on One of the Parallel Lines With Unbalanced Prefault Conditions.

D. Cross-Country Faults (CCFs)

Fig. 12 shows the operating times of the local and remote relays for a CCF. The fault starts as an A-phase-to-ground fault located 80 percent from the local terminal of the parallel line of the system in Fig. 9. After 8 ms, a C-phase-to-ground fault occurs on the protected line located 80 percent from the local relay. R_F equals 250 Ω for both faults. The 67LQ elements, FPI logic, and 32IQ elements detect the fault in 18 ms, 75 ms, and 125 ms respectively.
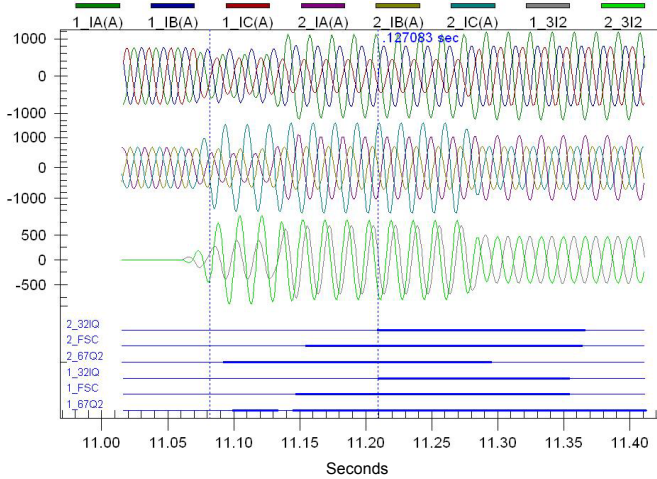

Fig. 12.   FPI, 32IQ, and 67Q Operating Times for a CCF. First, an A-Phase-to-Ground Fault Occurs on the Parallel Line. After 8 ms, a C-Phase-to-Ground Fault Occurs on the Protected Line. R_F Equals 250 Ω for Both Faults.

Now, we increase R_F to 450 Ω. The 32IQ elements do not operate for this fault because of the first unbalanced fault. For this reason, the 32IQ elements do not appear in Fig. 13. Table III shows the operating times of the 67Q, FPI, and 87LQ local and remote elements. We set 87_Slope = 0.2.

TABLE III.   OPERATING TIMES OF 67Q, FPI, AND 87LQ ELEMENTS

	Local (ms)	Remote (ms)
67Q	83	23
FPI	96	94
87LQ	148	158

We note that for both CCFs the total current FPI provides reliable phase selection information. The 87LQ and 67Q elements provide better R_F coverage than the 32IQ element for unbalanced prefault conditions. We also combine the 67Q elements with the FPI logic to trip the correct phase in SPT applications.
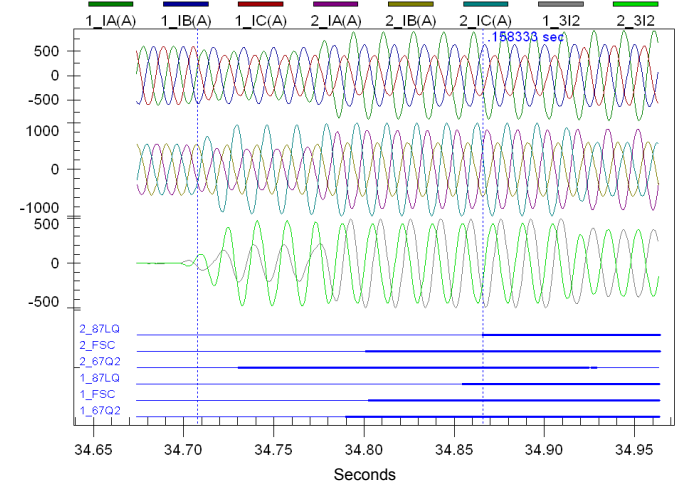

Fig. 13.   FPI, 87LQ, and 67Q Operating Times for a CCF. First, an A-Phase-to-Ground Fault Occurs on the Parallel Line. After 8 ms, a C-Phase-to-Ground Fault Occurs on the Protected Line. R_F Equals 450 Ω for Both Faults.

IV. POWER SWING AND OUT-OF-STEP DETECTION

Traditional power swing and OOS detection devices use voltage and current measurements that these devices acquire at a particular power system location.

The Clarke Diagram [10] in Fig. 14, shows the load impedance, Z_λ, in a two-machine system for $|E_A/E_B| = 1.1$ and $\delta = 70°$. The diagram also shows the trajectory of Z_λ on the impedance plane for $|E_A/E_B| = 1.1$. This voltage ratio and the impedance between the two sources define the impedance trajectory. E_A and E_B are the electromotive forces of the two machines, and δ is the angle between E_A and E_B.
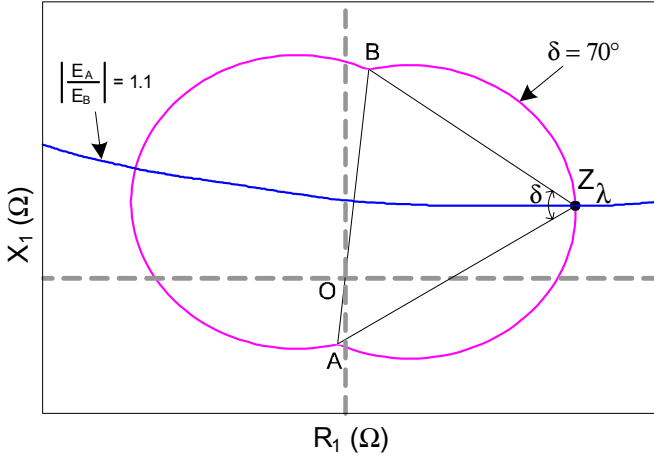
Fig. 14.   Load Impedance Trajectory on the Impedance of Plane for $|E_A/E_B| = 1.1$.

Line relays include an OOS element that uses local information to monitor impedance trajectory for discrimination between power swings and fault conditions [11]. When this OOS element detects power swing conditions, it blocks the distance elements. The OOS element requires the apparent impedance to enter dedicated impedance characteristics. We want to detect power swings before the apparent impedance enters the OOS impedance characteristic.

The Power Swing Relay [12] uses a different OOS detection method. It determines δ from positive-sequence voltages and positive-sequence currents that the relay measures at one location. To calculate the voltage at the remote end, the power swing detection algorithm requires network parameter and network topology information. This relay calculates the first and second derivatives of the angle difference, δ, to identify unstable swing conditions.

Another approach to δ calculation is to use synchrophasors from devices located close to generators [13]. This approach does not require network parameter and network topology information.

We now describe a synchrophasor-based approach that calculates slip frequency and acceleration to identify power swings and OOS conditions. The change of δ with respect to time defines the slip frequency, S_f, and the change of slip frequency with respect to time defines the acceleration, A_f, between the two system areas.

A. Power Swing Detection (PSD)

The PSD algorithm uses the positive-sequence voltage angles that relays with synchrophasor measurement capabilities acquire at two different power system buses to calculate δ between these buses. Then, the algorithm determines S_f and A_f between the two system areas. The relay running the PSD algorithm calculates the absolute values of S_f and A_f at constant intervals according to the synchrophasor message rate. Fig. 15 shows the block diagram of the PSD algorithm.
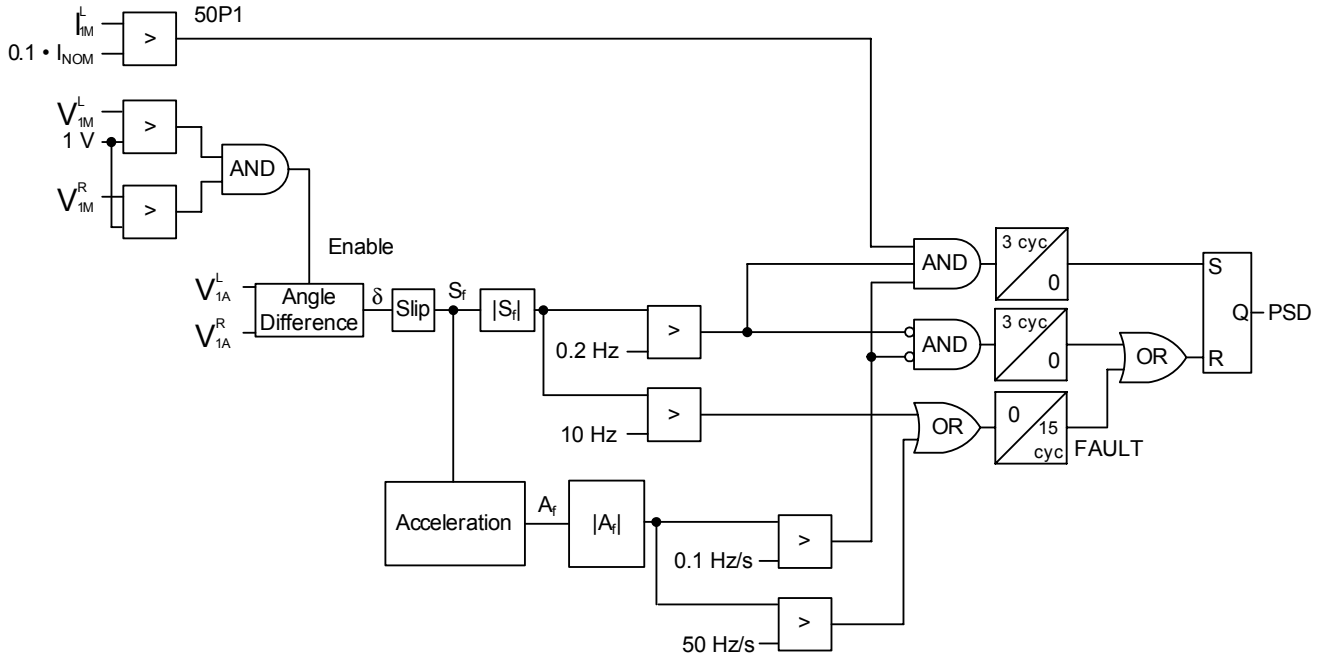

Fig. 15.   Synchrophasor-Based Power Swing Detection Logic.

The algorithm enables the angle difference calculation when all of the following operating conditions exist:

- Local positive-sequence voltage magnitude, V_{1M}^{L}, is greater than 1 V secondary.
- Remote positive-sequence voltage magnitude, V_{1M}^{R}, is greater than 1 V secondary.

When local positive-sequence current magnitude, I_{1M}^{L}, is greater than $0.1 \bullet I_{NOM}$, $|S_f|$ is greater than 0.2 Hz, and $|A_f|$ is greater than 0.1 Hz/s for three cycles, the algorithm asserts the power-swing detection bit, PSD. The PSD bit assertion indicates the existence of a power swing condition. The PSD bit deasserts when any of the following conditions occur:

- $|S_f|$ is greater than 10 Hz
- $|A_f|$ is greater than 50 Hz/s
- $|S_f|$ is less than or equal to 0.2 Hz and $|A_f|$ is less than or equal to 0.1 Hz/s for three cycles

Relay engineers can modify these thresholds according to their applications.

B. Predictive Out-of-Step Tripping (OOST)

The OOST element characteristic [12] in Fig. 16 uses (6) to define the power system unstable region. This characteristic identifies unstable swings before the OOS condition occurs, allowing the system protection scheme to take immediate remedial actions.

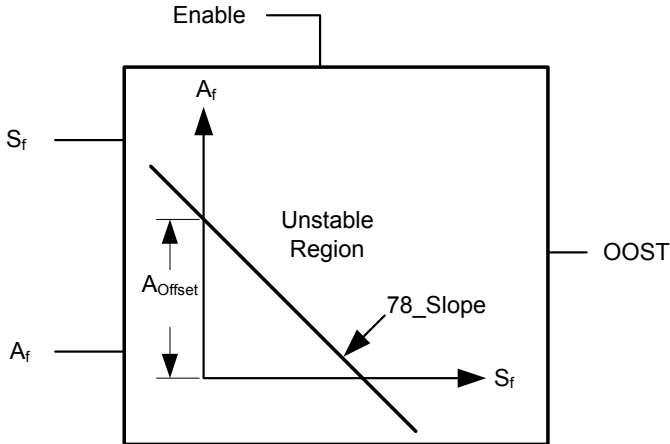$$A_f > 78\_Slope \bullet S_f + A_{Offset} \qquad (6)$$

Fig. 16. OOST Characteristic Using Slip and Acceleration Information to Detect Unstable Swings.

C. Out-of-Step Detection (OOSD)

OOSD element assertion indicates machine pole slip events. The OOSD logic in Fig. 17 compares the absolute value of the calculated angle difference with the OOS threshold, OOSTH. This threshold defines the Angle Difference Operating Region (ADOPR) in Fig. 18. This logic monitors whether the Angle Difference Operating Point (ADOP) crosses this region. When ADOP crosses the ADOPR region, the logic asserts the OOSD bit to indicate the OOS occurrence. Note that ADOP can cross this region from the right or

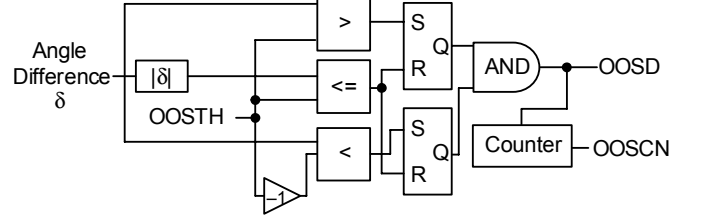from the left. The OOSD bit feeds the OOS counter (OOSCN) to track the number of OOS events.

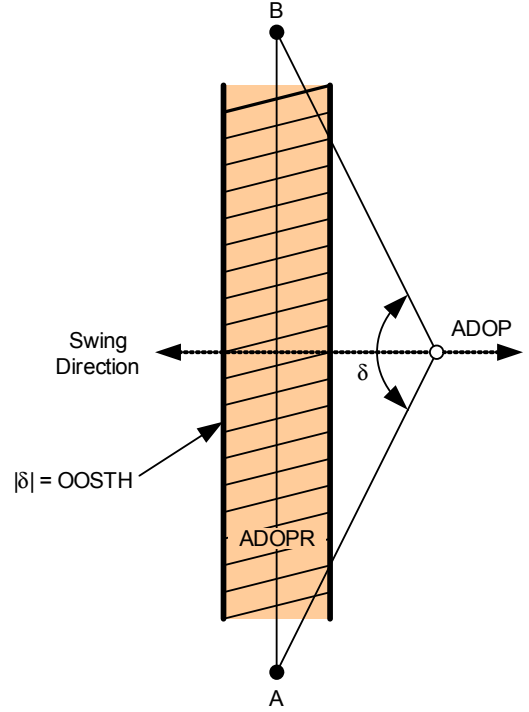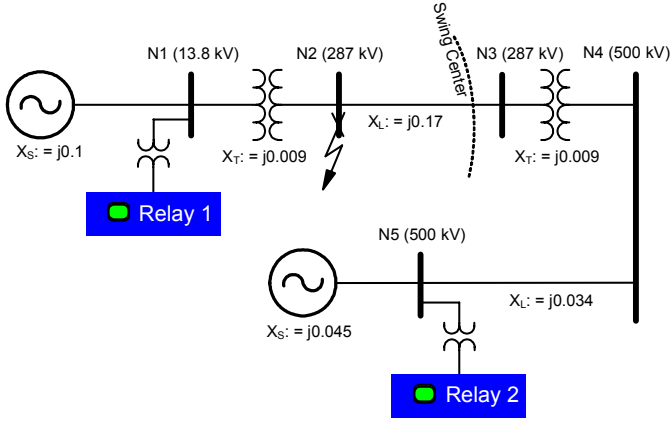Fig. 17. OOSD Logic Uses Angle Difference Information to Identify Out-of-Step Conditions.

Fig. 18. Angle Difference Operating Region.

V. POWER SWING AND OUT-OF-STEP DETECTION ALGORITHM PERFORMANCE

We used the two-machine RTDS power system model in Fig. 19 and the MATLAB® power swing and OOS detection algorithms running at 60 messages per second to analyze PSD, OOST, and OOSD logic performance.

Fig. 19. Two-Machine Power System Model to Illustrate PSD, OOST, and OOSD Element Performance During Power Swing and Out-of-Step Conditions.

A. Power Swing Detection (PSD)

At 0.5 seconds, the system has a fault for 7.25 cycles at bus N2. After the fault is removed, the power swing condition begins: $|S_f|$ is greater than 0.2 Hz, $|A_f|$ is greater than 0.1 Hz/s, and the PSD bit asserts at 0.94 seconds (see Fig. 20). The PSD element detects the swing condition 2.93 seconds before the machine poles slip.

B. Predictive Out-of-Step Tripping (OOST)

The delta-slip plot in Fig. 21 shows the angle difference and slip calculations from 0.81 to 3.87 seconds. Three seconds after fault inception, δ is greater than 90°, and the swing becomes unstable. The slip-acceleration plot in Fig. 22 shows the slip and acceleration calculations from 3.39 to 4.79 seconds together with the OOST element characteristic. In this example, we set 78_Slope = –15 and A_{Offset} = 7. The OOST element detects the OOS condition 3.16 seconds after fault inception and 0.22 seconds before the machine poles slip (see Fig. 20). An angle δ greater than 90° supervises this element to increase scheme security.
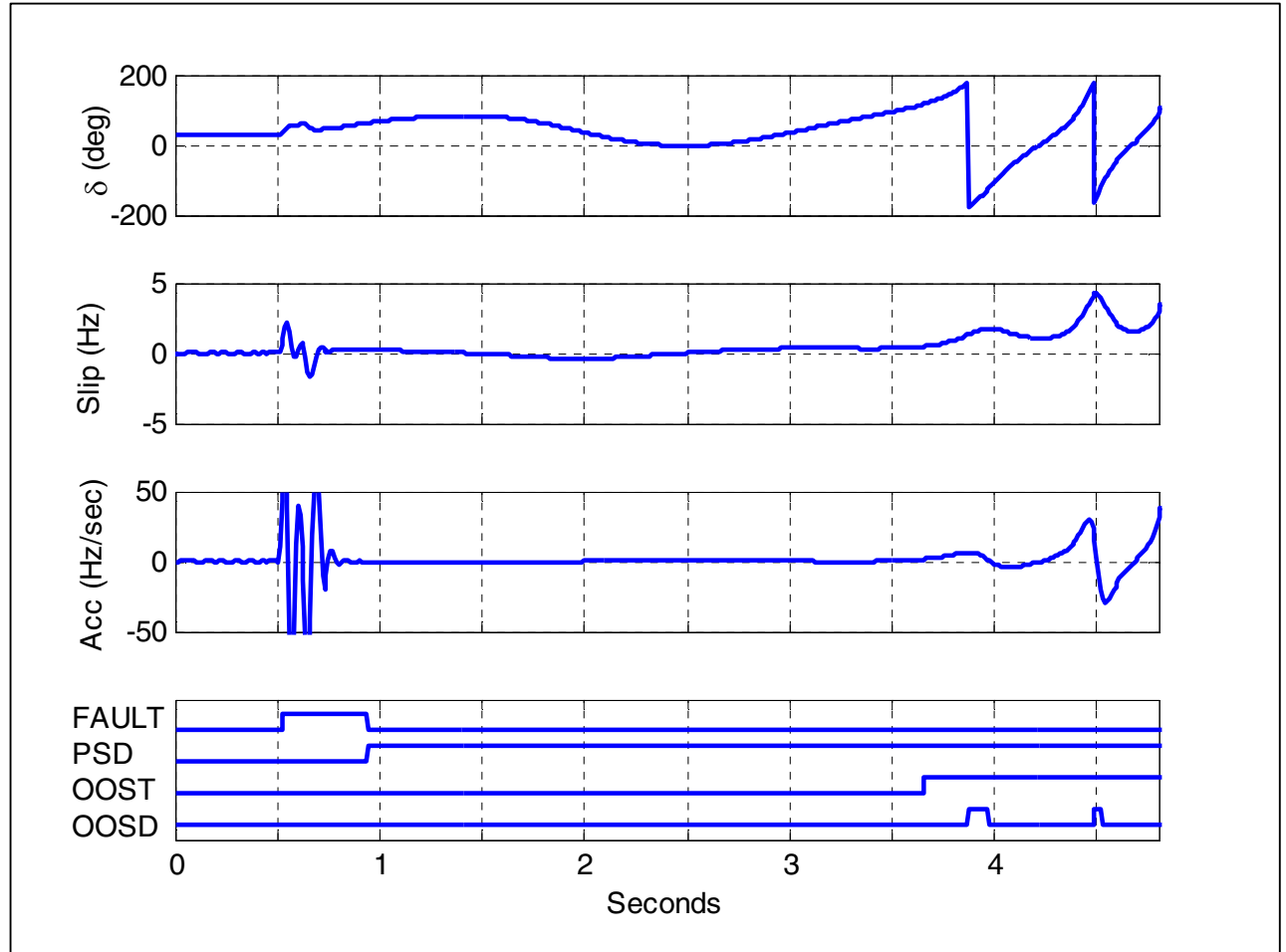.

Fig. 20. Angle Difference, Slip, Acceleration, and Digital Bits for an Unstable Swing after a 7.25-Cycle Fault at Bus N2.

C. Out-of-Step Detection (OOSD)

The OOSD bit asserts at 3.88 seconds when the OOS condition occurs (see Fig. 20). The angle difference trajectory in Fig. 23 illustrates when ADOP enters and leaves ADOR. In this example, OOSTH = 120°.
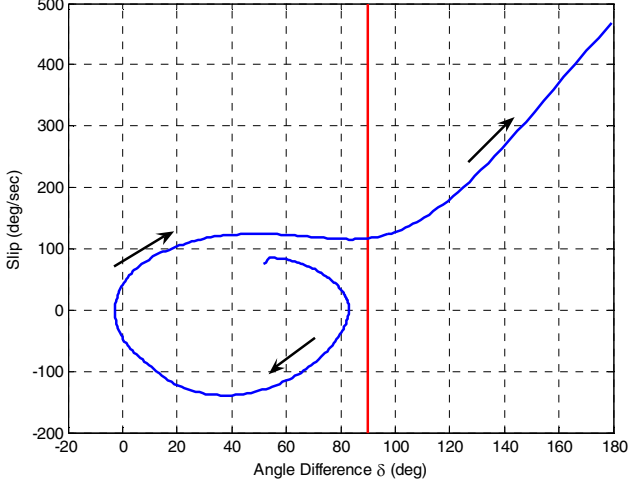

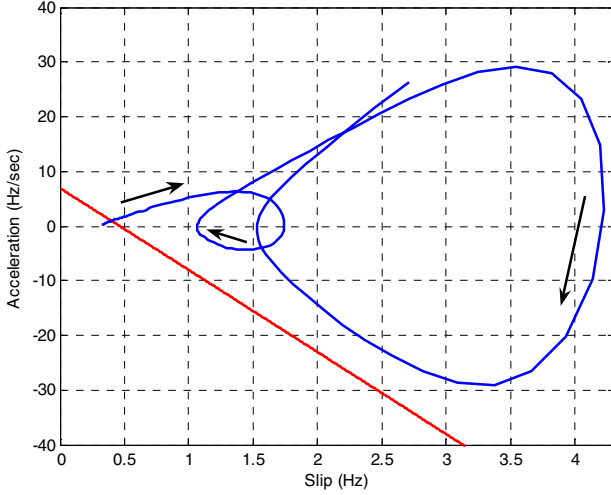Fig. 21.   The System Becomes Unstable When δ is Greater Than 90°.

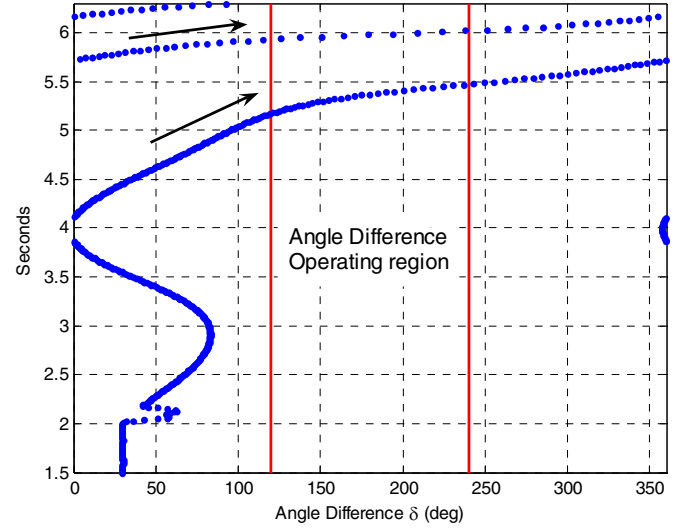Fig. 22.   OOST Characteristic Using Slip and Acceleration Information Determines Unstable Swing Condition

Fig. 23.   ADOP Trajectory Indicates When the OOS Condition Occurs.

VI. POWER SWING AND OUT-OF-STEP DETECTION RELAY PERFORMANCE

The following results show performance for OOS algorithms implemented in a two relay protection system using programmable logic. Section IV describes these algorithms in more detail.

The test system in Fig. 19 simulates swing conditions. Protective relays at bus N1 and N5 exchange synchrophasor data (positive-sequence voltage angle) and run the OOS algorithms 20 times per second using peer-to-peer relay communications.

We applied a three-phase fault at bus N2 for 7.25 cycles to start the power swing, as we did in Section V. Fig. 24 shows the three-phase voltages at each bus. Note that during the pole-slip period the voltages drop to nearly zero at buses N3 and N4. These buses are close to the swing center of the system.
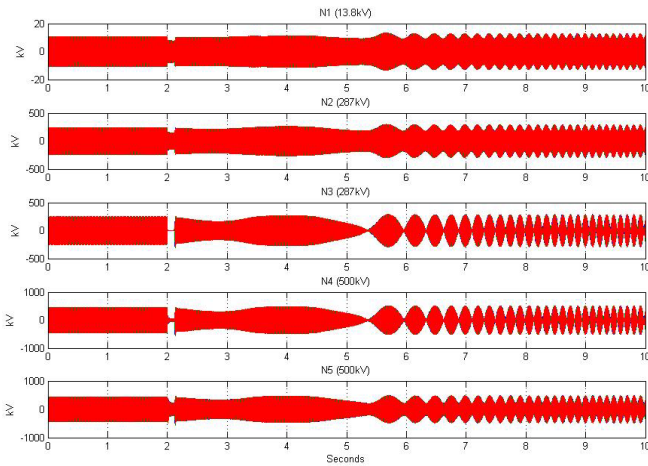
Fig. 24. Instantaneous Three-Phase Voltages at Each Bus on the Test System.

Fig. 25. Relay Oscillography Showing the Power Swing Detection Element Response for the System Oscillations.

Fig. 25 shows the relay oscillography at bus N1 triggered during the swing. Analog values include the three-phase voltages and the three-phase currents. Digital values include PSD, OOST, and OOSD. The PSD bit asserted 3 seconds before the first pole slip when the OOSD bit asserted. The OOST element detected the slip condition 0.23 seconds before the first pole slip, providing adequate time for remedial action.
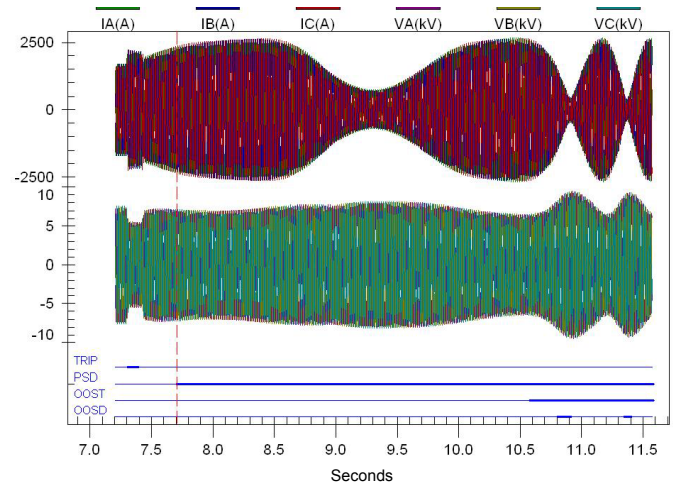
To illustrate the angle difference, slip, and acceleration analog values that the relay calculated, we included the analog values in the synchrophasor output message. We used a synchrophasor visualization tool to obtain the results in Fig. 26. These results are similar to the calculations shown in Fig. 20.
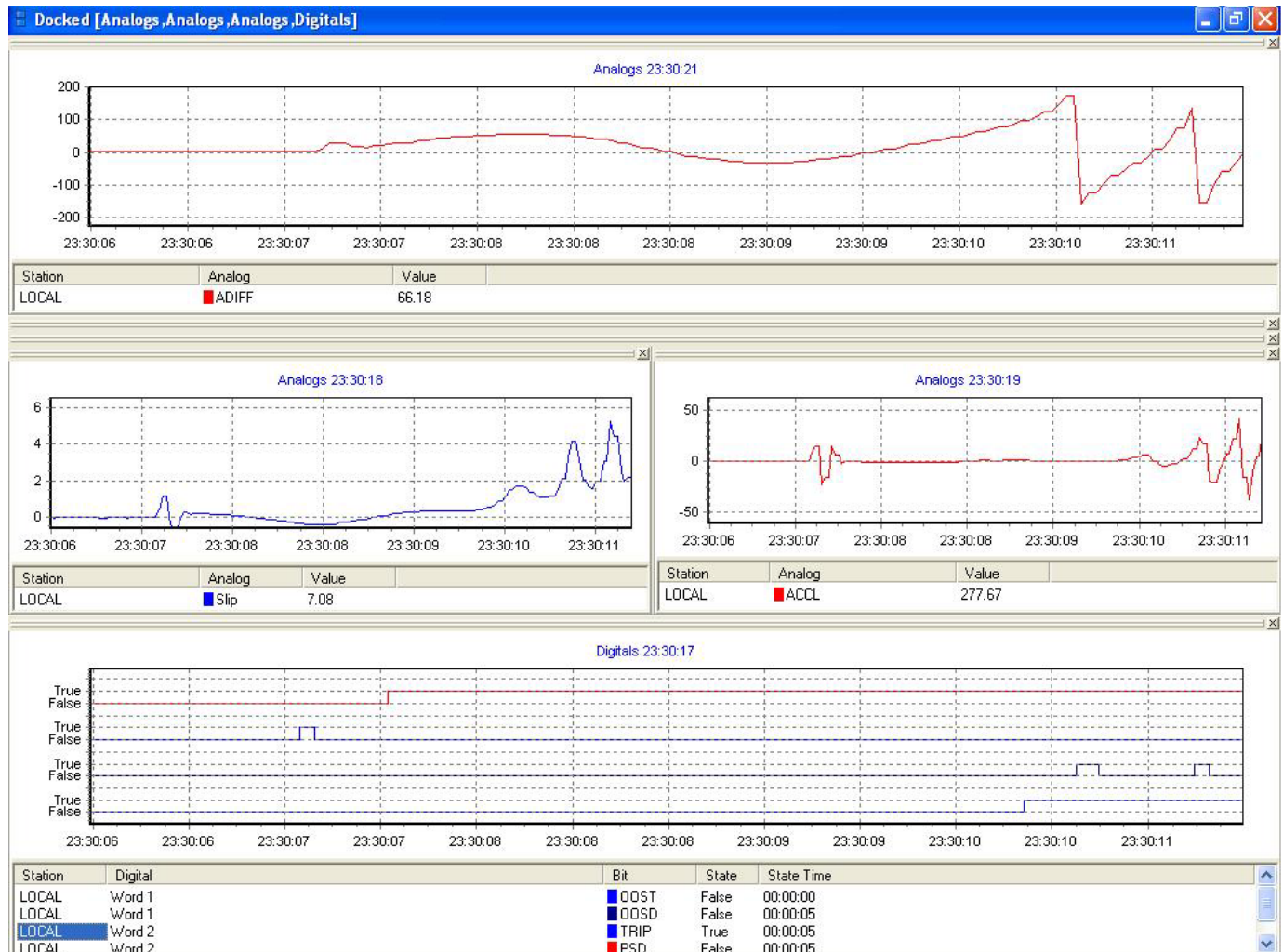

Fig. 26. Angle Difference, Slip Frequency, Acceleration Relay Calculations, and PSD, OOST, OOSD Element Operation.

VII. Conclusions

1. Synchrophasor-based protection complements primary distance protection schemes, provides backup protection, and does not require voltage information. The latter capability allows the relay to protect the line during loss-of-potential conditions.

2. Negative-sequence current directional and differential elements together with total current faulted phase identification detect high-resistance faults without compromising phase selectivity. These elements have minimum communication bandwidth requirements.

3. Negative-sequence current differential elements provide sensitive protection with unbalanced pre-fault conditions.

4. Communications channel asymmetry does not affect the operating and restraint quantities of the synchrophasor-based current differential element.

5. PSD, OOST, and OOSD elements do not require power system network parameter and topology information to calculate angle difference, slip frequency, and acceleration between two system areas.

6. Synchrophasor-based protection and monitoring require reliable communications and reliable time information.

7. Time-aligned current and voltage measurements acquired at different power system locations improve performance of protection and power swing detection algorithms.

VIII. References

[1] G. Benmouyal, E. O. Schweitzer, III, A. Guzmán, "Synchronized Phasor Measurement in Protective Relays for Protection, Control, and Analysis of Electrical Power Systems," in *2002 29th Annual Western Protective Relay Conference Proceedings*.

[2] E. O. Schweitzer III and J. Roberts, "Distance Relay Element Design," in *1992 19th Annual Western Protective Relay Conference Proceedings*.

[3] E. Martinez et al., "Using Synchronized Phasor Angle Difference for Area-Wide Protection and Control," in *2006 33rd Annual Western Protective Relay Conference Proceedings*.

[4] J. B. Roberts and D. Tziouvaras, "Fault Type Selection System for Identifying Faults in an Electric Power System," US Patent 6,525,543, Feb. 25, 2003.

[5] A. R. van C. Warrington, *Protective Relays: Their Theory and Practice*, vol. 1 London: Chapman and Hall, 1974, p. 106.

[6] F. Calero and W. A. Elmore, "Current Differential and Phase Comparison Relaying Schemes," in *1992 19th Annual Western Protective Relay Conference Proceedings*.

[7] *IEEE Synchrophasors for Power Systems*, IEEE Standard C37.118-2005.

[8] K. C. Behrendt, "Relay-to-Relay Digital Logic Communication for Line Protection, Monitoring, and Control," in *1997 51st Annual Georgia Tech Protective Relaying Conference Proceedings*.

[9] G. Benmouyal, "The Trajectories of Line Current Differential Faults in The Alpha Plane," in *2005 32nd Annual Western Protective Relay Conference Proceedings*.

[10] E. Clarke, *Circuit Analysis of AC Power Systems*, vol. II New York: Wiley and Sons, 1950, pp. 335–343.

[11] D. Hou, A. Guzman, and J. Roberts, "Innovative Solutions Improve Transmission Line Protection," in *1997 24th Western Protective Relay Conference Proceedings*.

[12] E. O. Schweitzer III, T. T. Newton, and R. A. Baker, "Power Swing Relay Also Records Disturbances," in *1986 13th Annual Western Protective Relay Conference Proceedings*.

[13] V. Centeno, J. de la Ree, A. G. Phadke, G. Michel, R. J. Murphy, R. O. Burnett, Jr., "Adaptive Out-of-Step Relaying Using Phasor Measurement Techniques," *Computer Applications in Power, IEEE*, Vol. 6, No. 4, pp. 12–17, Oct 1993.

IX. Biographies

Armando Guzmán received his BSEE with honors from Guadalajara Autonomous University (UAG), Mexico, in 1979. He received a diploma in fiber-optics engineering from Monterrey Institute of Technology and Advanced Studies (ITESM), Mexico, in 1990, and his MSEE from University of Idaho, USA, in 2002. He served as regional supervisor of the Protection Department in the Western Transmission Region of the Federal Electricity Commission (the electrical utility company of Mexico) in Guadalajara, Mexico for 13 years. He lectured at UAG in power system protection. Since 1993 he has been with Schweitzer Engineering Laboratories, Inc. in Pullman, Washington, where he is presently Research Engineering Manager. He holds several patents in power system protection and metering. He is a senior member of IEEE and has authored and coauthored several technical papers.

Mangapathirao "Venkat" Mynam received his MS in Electrical Engineering from the University of Idaho in 2003 and a Bachelors in Electrical and Electronics Engineering from Andhra University College of Engineering, India, in 2000. He is presently working as a Research Engineer with Schweitzer Engineering Laboratories, Inc. He is a member of IEEE.

Greg Zweigle earned his BS in Physics and MS in Electrical Engineering from Northwest Nazarene University and Washington State University, respectively. He is presently a Principal Research Engineer at Schweitzer Engineering Laboratories in Pullman, Washington. He holds patents in the areas of power systems, signal processing, and data compression and is a member of the IEEE and the ACS.